IEEE Access
Multidisciplinary ⋮ Rapid Review ⋮ Open Access Journal

Received 21 September 2023, accepted 26 September 2023, date of publication 29 September 2023,
date of current version 4 October 2023.

Digital Object Identifier 10.1109/ACCESS.2023.3320794

RESEARCH ARTICLE

A Multiaxis Force Sensor Based on Pre-Strained Piezoresistive Film Strips

SHICHAO YUE[1], (Member, IEEE), MINZHI XU[1], YANPENG GU[1], AND WALIED MOUSSA[2]
[1]Mechanical Engineering Department, Southeast University, Nanjing, Jiangsu 211189, China
[2]Mechanical Engineering Department, University of Alberta, Edmonton, AB T6G 2G2, Canada

Corresponding author: Shichao Yue (syue@seu.edu.cn)

This work was supported in part by the Natural Scientific Funding of Jiangsu Province under Grant BK20200401, and in part by the Fundamental Research Funds for Central Universities of China under Grant 1102007138.

ABSTRACT Soft multi-axis force sensors are essential in automation and robotic manipulations for dexterous applications. Carbon-based composites are quality candidates for sensing elements of soft multi-axis force sensors due to its piezoresistivity originated from electron tunneling effect. However, low cost and fast-prototyped soft multi-axis force sensors based on tunneling effect of carbon-based composites are still in their infant. This work investigated a soft multi-axis forces sensor utilizing Velostat film strips as the core sensing elements. A unique serpentine structure of Velostat strips has been designed and implemented as piezoresistors for the soft force sensor. The sensitivity of the proposed multi-axis force sensor has been characterized in x, y and z directions. Experimental results show that the sensor can achieve 2.1%/N and 2.2%/N in x and y axis, and 4.2%/N in z axis, respectively. The force sensor has been implemented in dexterous manipulations with a robotic gripper as the proof-of-concept, which demonstrates great potential for multi-axis force sensing applications.

INDEX TERMS Velostat, multi-axis force sensor, piezoresistivity, robotic gripper.

I. INTRODUCTION

Multi-axis force sensors involve significant aspects in automation industries [1], biomedical engineering [2], space engineering, packaging equipment, robotics [3], etc. The majority of multi-axis force sensors are built with rigid material such as silicon chips [4], [5] or metal embodiment [6], and used with the end effector while measuring contact force during manipulation/handling operations. However, as dexterous handling and precise gripping demand force feedback from end effectors, intelligent applications need multi-axis force sensors to be manufactured with soft materials to fulfill manipulation requirements for delicate products, for instance, in the food processing industry, customized artworks, slender parts assembly, etc. Therefore, high performance, low cost, and adequate form factor have been the primary pursuit for the development of the soft multi-axis force sensor.

The associate editor coordinating the review of this manuscript and approving it for publication was Shuo Sun.

A. SENSING FUNDAMENTALS OF MULTI-AXIS FORCE SENSOR

Similar to general rigid force sensors, soft force sensors can work based on common fundamentals such as piezoresistivity, capacitance changes, magnetic field variations, optical properties [7], etc. Noda et al. realized a multi-axis force sensor by embedding silicon piezoresistors inside PDMS. Liang et al. investigated a capacitive tactile sensor array for robotic applications with truncated pyramid structures [8]. Nasab et al. developed a multi-axis force sensor based on the hall effect, achieving a resolution of mN [9]. For robot-human collision detection, a compliant fiber optics-based multi-axis force sensor was developed with good linearity [10].Piezoresistive sensors have good linearity and simple conditioning electronics but need more caution on temperature drift. Capacitive sensors are quite immune to temperature fluctuations, however, they require more complex circuits to process the output signals [11]. Magnetic force sensors are usually bulky due to the permanent magnetic block and the sensing coils. With off-the-shelf magnetic field

TABLE 1. Comparison between the proposed work and recently published sensors based on Velostat.

Force type	Measurement range	Cell size	Application field	Reference
Pressure	15 N	7×7 mm ^{2}	Biomedical Engineering Foot pressure	Ref. [13]
F_z	3.5 N	25 mm^2	Tactile	Ref. [14]
Pressure	130 KPa	D $\simeq$10 mm	Biomedical Engineering Foot pressure	Ref. [15]
Pressure	0.5N	2.5 $\times$2.5 mm	Intelligent system Object recognition	Ref. [16]
Pressure	110 KPa	D $\simeq$ 2 mm	Biomedical Engineering Prosthetic Socket	Ref. [17]
Pressure location	60 KPa	10 mm	Biomedical Engineering Stroke monitoring	Ref. [18]
F_z	200 N	D $\simeq$5 mm	Intelligent system Object recognition	Ref. [19]
Pressure	300 KPa	3.5 mm	Intelligent system Object recognition	Ref. [20]
F_x, F_y, and F_z	10 N,10 N, and 10N	20$\times$20$\times$10 mm	Robotics Gripper	This work

measurement devices, a magnetic-device-based multi-axis force sensor is simple to implement but prune to ambient magnetic interferences. Optical sensors demonstrate good flexibility in terms of optical fibers [12], although, suffer from bulky and relatively expensive optic-electronic modules. Therefore, piezoresistive force sensors exhibit advantages of ease in the implementation, physical simplicity, and cost-effectiveness, that still gain numerous tractions in terms of sensor investigations.

B. PIEZORESISTIVE MULTI-AXIS FORCE SENSORS

Compliant piezoresistive force sensors can be developed with doped silicon, however, embedded inside other flexible substrates as ultra-thin strips [21]. Other piezoresistive force sensors utilize conductive properties of carbon black [22], liquid metal [23], carbon nanowires, silver nanowires [24], and single or multiple layers of graphene [25]. These various types of force sensors work based on percolation networks with aforementioned conductive fillers embedded inside elastomer substrates. Noticeably, the Velostat film has been a promising material candidate for investigating force sensors [19]. The sensing devices could be realized or prototyped quickly by cutting the Velostat into shape and combining the mesh with copper electrodes. Therefore, the Velostat film has been the choice of the proposed work for the sensing element of the multi-axis force sensor. Utilizing the high performance of piezoresistivity of Velostat for multi-axis force sensors will be of great advantage in terms of its sensitivity, flexibility, and low cost.

C. MULTI-AXIS FORCE SENSOR APPLICATIONS

With the advancement of automation, intelligent devices, and wearables, force sensors are required for numerous applications such as robotics [26], [27], prosthetics [25], human-machine interfaces [28], etc. Multi-axis forces sensors can be utilized at the robotic joint for more precise control with force feedback to enhance robotic manipulations. Specifically, Velostat-based force sensors have been implemented for various applications such as gripping, dexterous handling, rehabilitation, or tactile intelligent sensor array. Notably, due to the design of the sensor structure, the majority of the sensor array or sensors with Velostat strips are mainly specialized for detecting pressing forces [14], as refer to Table 1. Therefore, extending the multi-axis force sensing scheme to Velostat-based force sensors will be of great potential for force measurements and tactile applications.

The following of this work is organized as below: first, the sensor design is introduced with the schematic structure of the multi-axis sensor, demonstrating the geometry and elements layout of the soft sensor; Second, the piezoresistors have been discussed to unveil its pre-strain status for explaining its resistance change mechanism which is different comparing with its pressure sensing counterparts; Third, the process flow for manufacturing the force sensor has been provided and discussed. The following chapter introduces the bench-top test setup and characterization equipment for the Velostat-based force sensor. Finally, discussions on the test results and sensor performances are included in this work. Applications on robotic grippers with the proposed sensor have been demonstrated. And the dynamic response time of the sensor is elaborated with experimental results. To conclude, the multi-axis sensor based on Velostat showed feasibility for measuring multi-axis force, demonstrating great potential for industrial or intelligent applications.

II. SENSING MECHANISM AND SENSOR IMPLEMENTATION

A. PERCOLATION THEORY AND PIEZORESISTIVITY

The piezoresistivity of the Velostat film can be explained by the percolation theory [29]. Carbon black particles are dispersed within the non-conductive polymer matrix in three major forms, which are primary particles, aggregate, and agglomerate [30]. For the three levels of dispersion, the conductivity of the carbon black mixed polymer matrix increases from non-conductive to conductive. The non-conductor

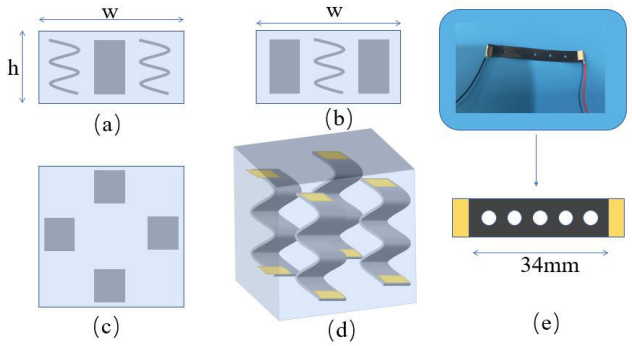

FIGURE 1. Schematic drawing of the sensor geometry and layout of piezoresistors.

to conductor transition of Velostat films resulting from percolation theory can be written as the equation 1 as follows [31]:

$$\sigma \propto (\phi - \phi_c)^t \tag{1}$$

where σ is the electrical conductivity of the Velostat, ϕ is the volume fraction between conductive filler and polymer matrix, ϕ_c is the volume fraction of percolation threshold, t is the power law index relating to the dimensionality of the conductive networks. With the percolation theory, the resistance of the Velostat film appears a decrement when a pressure force is applied. But, governed by the general piezoresistivity theory, the strain applied on a composite conductor leads to its change of resistance. This phenomenon is described by the equation 2 as below [32]:

$$\frac{\Delta R}{R} = (1 + 2\nu)\varepsilon + \frac{\Delta \rho}{\rho_0} \tag{2}$$

B. SENSOR DESIGN

The soft multi-axis force sensor is composed of two main parts: one is the sensor substrate which is made of PDMS cast inside a 3D printed mold for directly bearing the applied force; the other part is a group of four piezoresistors fabricated by the laser ablation with a piece of Velostat film, converting mechanical strain into electrical resistance changes. The schematic geometry of the force sensor has been portrayed in Fig. 1 to illustrate its form factor and piezoresistor configurations. Fig. 1 - (a), (b), and (c) indicate the front, side, and top-down views of the sensor. Fig. 1- (d) depicted the perspective view of the sensor to elaborate the how the four sensing elements are arranged spatially. Generally, the form factor of the sensor geometry can be reduced by utilizing a smaller mold template and narrower Velostat film strips. The geometry of the film strips can also be modified to get a specific length-width ratio to tune the initial resistance and sensitivity of the piezoresistor.

C. SENSING MECHANISM OF THE MULTI-AXIS FORCE SENSOR

Piezoresistive multi-axis force sensors can detect arbitrary directional force according to the outputs of multiple sensing elements. The four piezoresistors are embedded inside the PDMS substrate in a serpentine shape, which allows the piezoresistors to store pre-strain. This pre-strained shape of the piezoresistors alleviates their initial resistance to a higher level, equivalent to a stretched status of flat Velostat film strips. Forces applied to the four resistors result in resistance changes in the sensing elements. For instance, if a pressing force is applied on the top surface of the sensor, the resistance of the four piezoresistors would increase. If a shear force is applied on the sensor along the direction of pointing from R1 to R4, the resistance of the resistor R1 would decrease and the resistance of the piezoresistor R4 would increase. The resistance changes of the piezoresistors can be acquired for calculating the force asserted onto the sensor once the sensor is characterized with a known sensor. The characterization process has been elaborated in our previous work for a silicon-based force sensor [33]. The force calculation can be written in the form of equation 3:

$$\begin{Bmatrix} F_x \\ F_y \\ F_z \end{Bmatrix} = \frac{\Delta R}{R} \times S \tag{3}$$

D. FABRICATION OF THE VELOSTAT-BASED MULTI-AXIS FORCE SENSOR

The Velostat-based sensor is fabricated by following procedures: first, a piece of Velostat film was cut into rectangle strips by the laser ablation process (Qijun Laser Marker, setting power at 60 W, output of 70 %, pulse frequency of 20 KHz, scanning velocity at 500 mm/s, 1 time of laser scan). The laser ablation-affected zone inside the Velostat strip has been investigated by the scanning electron microscope (SEM) which would be discussed later. After sorting out the piezoresistive strips of Velostat film, about 50 mm of copper wire was cut and connected with each end of the piezoresistive film strips. The strips of the Velostat were connected to copper wires by thin bronze clamps formed with a crimper. To ensure the film strip was reliably connected, the resistance of the piezoresistors was measured by a multimeter. The Velostat film strips were bent and kept in the serpentine shape within a plastic mold, which was manufactured by a 3D printer with the material PLA. Then the PDMS solution mixed at a ratio of 1:10 was poured into the mold and cured for 45 minutes at the temperature of 60° C. To avoid the PDMS solution from leaking out of the PLA mold, the plasticine was applied to seal the bottom of the PLA mold. Eventually, the multi-axis force sensor was de-molded from the PLA case and ready for electrical tests and characterizations. The schematic process flow for making the soft multi-axis sensor has been plotted in Fig. 2.

E. CHARACTERIZATION AND TEST SETUP

The soft multi-axis piezoresistive force sensor was characterized by another multi-axis force sensor with a known sensitivity(Purchased from Epic Sensor Technology Inc.),

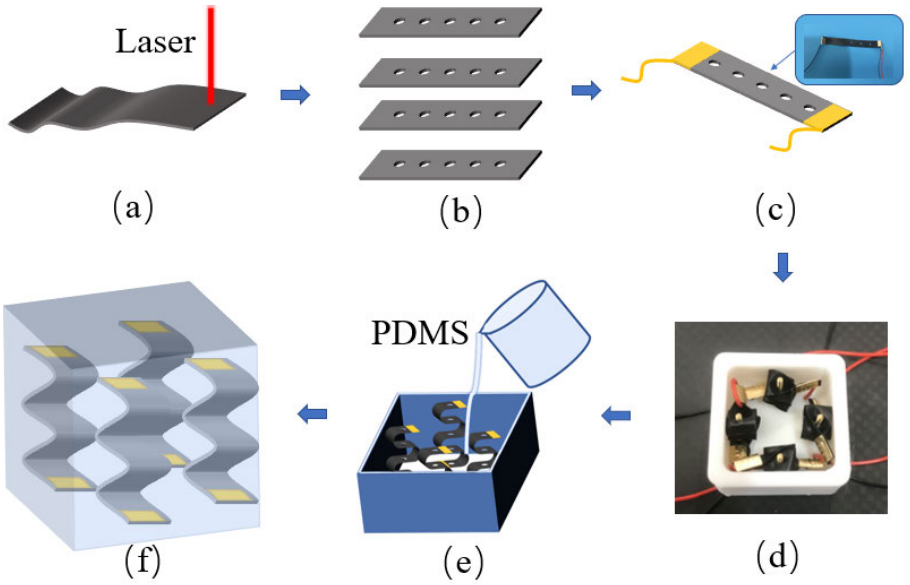

FIGURE 2. Process flow of fabricating the sensor.

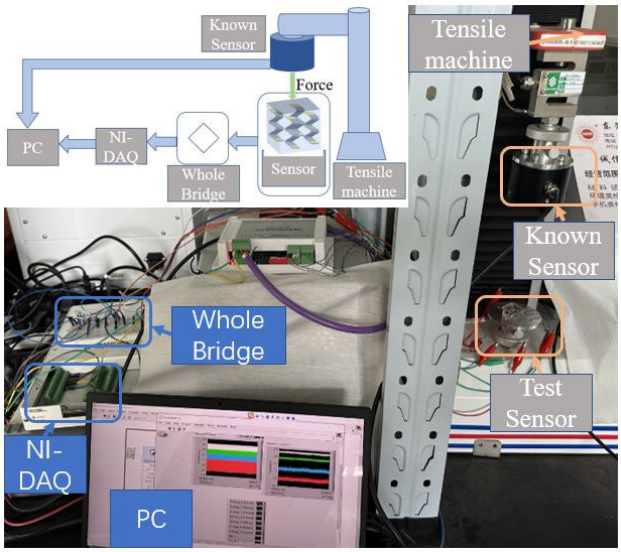

FIGURE 3. Test setup for the multi-axis force sensor.

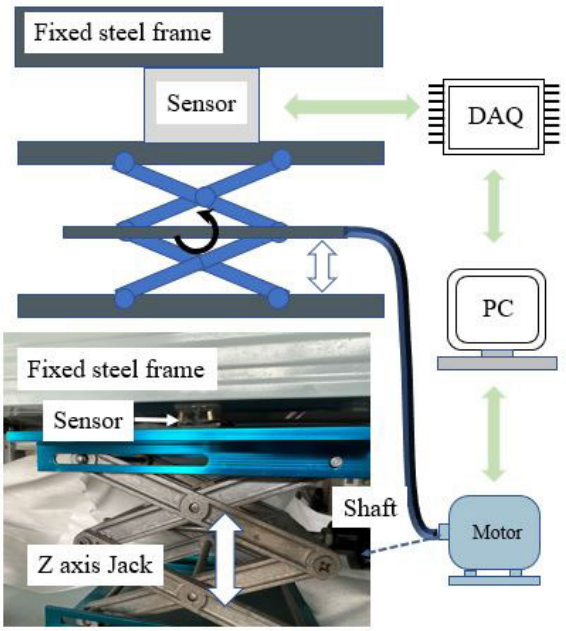

FIGURE 4. Test setup for repeated loads on the multi-axis force sensor.

which could be denoted as a standard sensor in the characterization procedure. To apply a known force on the soft sensor, the standard sensor was attached to a universal tensile machine. For characterizing multiple axes of the fabricated sensor, the force sensor was measured in the x, y, and z directions, respectively. The characterization setup was shown in Fig. 3.

As shown in Fig. 4, repeated loads have been applied on top of the multi-axis force sensor. The sensor was placed between a Z-axis movable jack and a fixed steel frame. The Z-axis movable jack was driven by a step motor connected to the desktop computer, which was also linked to the data acquisition card (DAQ). The collected data were analyzed in section III-C.

III. RESULTS AND DISCUSSIONS

A. MICRO-STRUCTURE ANALYSIS OF VELOSTAT FILM STRIPS

To further understand the conductive path which forms within the Velostat strips, scanning electron microscope(SEM) images were taken for investigating the micro-structures of

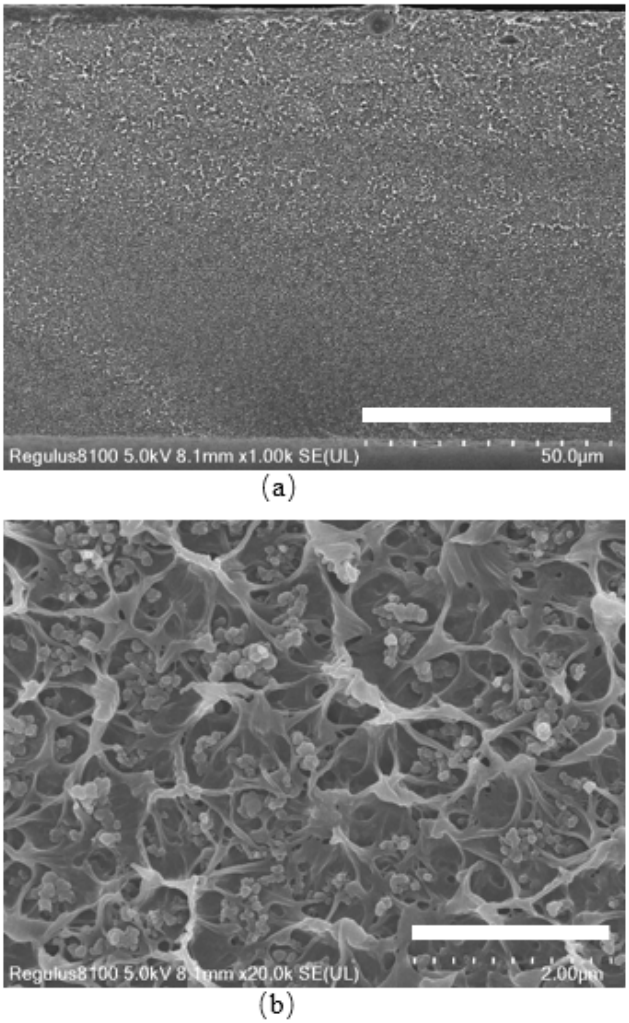

FIGURE 5. The SEM images of Velostat film strips (scale bar in a is 50 um, scale bar in b is 2um).

the Velostat films. The Velostat film strips were dipped into liquid nitrogen for 3 minutes and broken in the middle with two tweezers for exposing the cross-section perspective. The reason for using liquid nitrogen for breaking the film strip into parts was to acquire sharp cleavage in the film and to avoid external influences on the Velostat film structure. As shown in Fig. 5, which were film strip samples captured by the SEM. The scale bar indicated that the thickness of the Velostat film was around 100 um. The cryogenic breaking method for the thin film worked well in terms of getting a clean and sharp cleavage. Only a few hundred nanometers were affected by the laser ablation, which would not affect the initial resistance of the sensing element, considering the relatively small affected area compared with the intact area. In the SEM image, high-structure carbon particles could be seen clearly embedded inside the spongy polymer matrix, forming connected conductive networks with other carbon agglomerates. The size of a single carbon black particle was around 100 nm, and the size of agglomerates varied from a few hundred nanometers to less than one micrometer. The

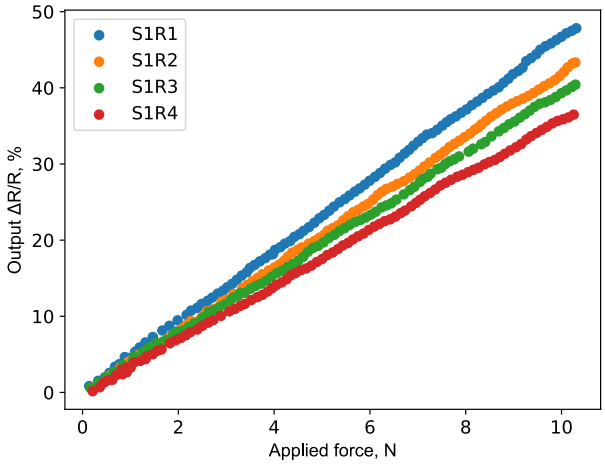

FIGURE 6. Sensor outputs with forces applied in z-direction.

microstructure of the Velostat can be interpreted as the reason for its piezoresistive behavior. The conductive path between different groups of agglomerates is shortened when the film is subjected to a compressive force, resulting in resistance reduction. On the contrary, the resistance of the film increases as the conductive paths rearranged to be longer or fewer under tensile forces.

B. ANALYSIS OF SENSOR CHARACTERIZATION

The multi-axis force sensor has been characterized with the sensitivity-known sensor(APDW-6D-70, purchased from Epic Sensor Technology Inc.) on a universal tensile machine. To test the sensor performance, a Wheatstone bridge circuit has been built to connect all the piezoresistive film strips. The output signals are collected using NI-USB-6225 data acquisition card(DAQ) through a USB cable to a computer. The post-processing of the original data is done with the Python package numpy. First, the sensor has been characterized in the Z-direction. The sensor has been applied with various amounts of force by a cylinder indenter with a diameter of 20mm. The resistance changes against applied force have been plotted in Fig. 6. The data show good linearity of the fabricated sensor. The sensitivity of the piezoresistive sensor in the Z-axis is about 4.2%/N. About 0.5% discrepancy existed among the four piezoresistive film strips, which could be accounted for by the non-uniformity of bulk film and geometry differences caused by the laser ablation process.

Second, the characterization for shear forces in the x and y directions is done by applying forces onto the soft sensor with a customized fixture and placing the sensor vertically as referred to in our previous work [34]. The shear force is applied along the surface of the multi-axis force sensor. The output data of the sensor performance in the x-direction are shown in Fig. 7. Both resistors S1R1 and S1R4 showed good linearity. About 0.5% crosstalk appeared from resistors S1R2 and S1R3, which can be explained by the relatively large width of the film strips compared with the sensor geometry.

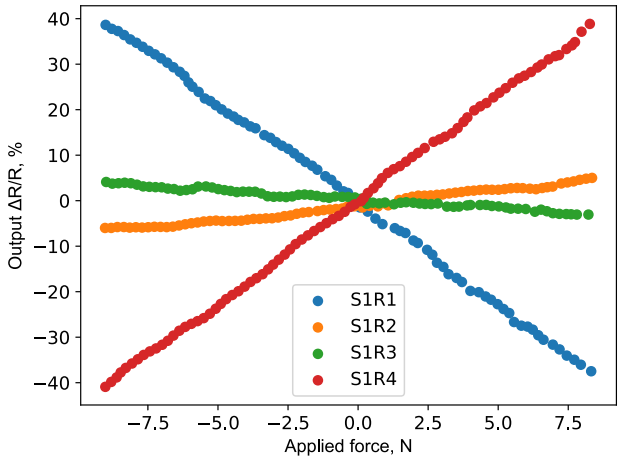

FIGURE 7. Sensor tests for shear force in X-direction.

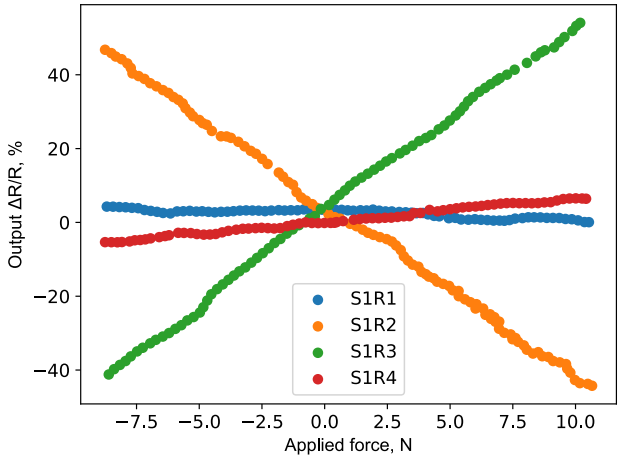

FIGURE 8. Sensor tests for shear force in Y-direction.

As applying force in the direction pointing from the location of S1R1 to S1R4, the outputs from S1R1 decreased from about zero to -39.5% and outputs from S1R4 increased from about zero to 41%, respectively. The shear force sensitivity in the x-axis is calculated to be around 2.1%/N.

Moreover, the sensor performance in the y-axis has also been characterized by applying a shear force in the direction pointing along the axis from S1R3 to S1R2, as shown in Fig. 8. The shear sensitivity of the multi-axis force sensor in y-axis is characterized as 2.2%/N. The discrepancy between the x and y axis in terms of sensor sensitivity are deemed as the misalignments for the piezoresistors placements, geometric variations caused by fabrication, and potential test fixture misalignments. Noticeably, the crosstalk of sensing elements S1R1 and S1R4 are not leveled at zero position, which is caused by zero offset during voltage data processing.

C. SENSOR FUNCTION TESTS

To demonstrate the sensor functions in the z-axis, the piezoresistive sensor was tested by pressing its surface three times with one finger. The outputs from the four

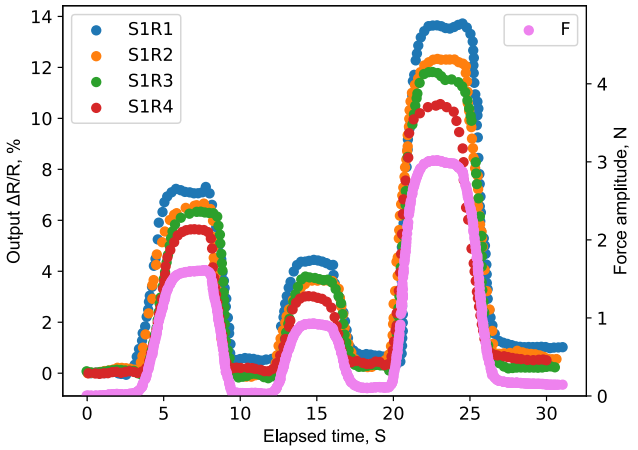

FIGURE 9. Sensor tests for applying pressing forces.

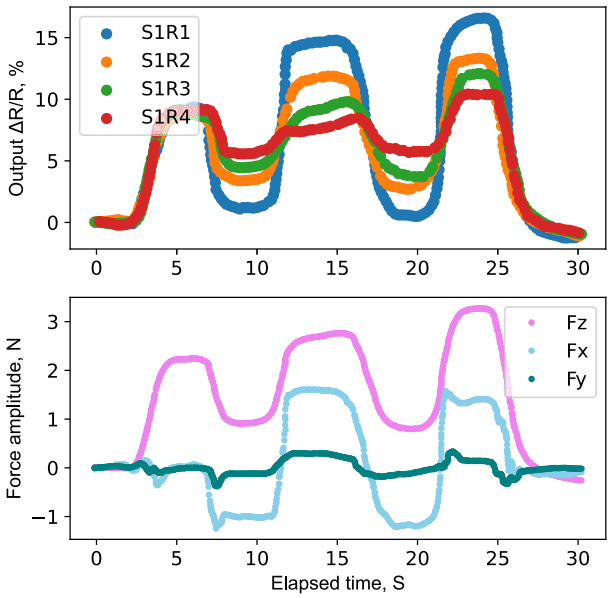

FIGURE 10. Sensor tests for applying rubbing forces.

piezoresistors are illustrated in Fig. 9. As applied pressure on top of the sensor, resistance changes are collected from the piezoresistors. The calculated forces according to previous characterizations are depicted in the figure marked against the secondary axis on the right. Noticeably, discrepancies among four piezoresistors appear larger than what is plotted in the characterization procedures. This can be interpreted as the uneven top surface of the sensor when applying force manually with a finger, which results in shear data shown in the output.

To demonstrate the shear force measurement function of the sensor, the piezoresistive sensor has been pressed and rubbed between the thumb and index finger. The sensor performance is shown in Fig.10. The manipulation started with pressing the sensor, then the surface of the sensor was rubbed along the direction from S1R1 to S1R4 and reversed. The rubbing motion was repeated four times after the pressing

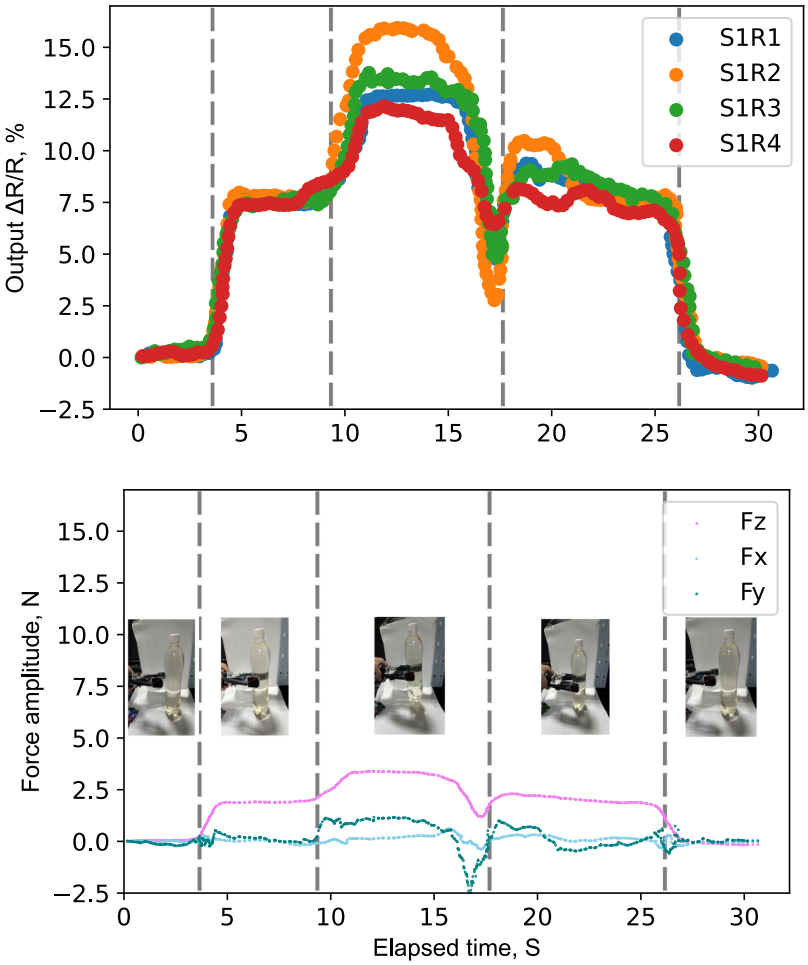

FIGURE 11. Multi-axis force sensor applied in a robotic gripper for grasping tests.

motion. Clearly shown in the outputs, as the sensor was pressed, the sensor resistance changes increased from the four piezoresistors with a similar amount. As the rubbing motion happened, shear forces were added to the sensor. Piezoresisitors S1R1 and S1R4 sensed the shear force and demonstrated resistance change discrepancies. Specifically, the outputs from S1R1 were lower than the outputs from S1R4 in the second plateau region. As the rubbing motion was applied in the opposite direction, which was from S1R4 to S1R1, the resistance changes from S1R1 were much higher than what was from S1R4. With the rubbing motion applied in alternating directions, the resistance changes from piezoresistors S1R1 and S1R4 demonstrated similar alternations trends in terms of increments and decrements as depicted in Fig. 10. Noticeably, the outputs from S1R2 and S1R3 also had a trend of peak alternations during the rubbing tests. This demonstration indicated that the multi-axis force sensor had good capability to sense pressing force and shear force simultaneously.

To introduce the application potentials of the multi-axis force sensor, the piezoresistive sensor was applied on the tip of a motorized robotic gripper. One step motor provided driving force for the robotic gripper, of which two fingers were connected by a four-bar mechanism. The gripper was held to reach and grasp a plastic bottle filled with dyed water. The outputs of the sensor were collected and plotted in Fig. 11. Before the gripper closed its two fingers, the resistance changes of the four piezoresistors remained to be zero. Once the grippers started touching the water bottle, resistance changes from the sensor increased and plateaued at around 2.5N as the gripper stopped squeezing the bottle. The robotic gripper was lifted together with the water bottle. A slight increase in resistance from four piezoresistors showed up in the data, which can be accounted for by the weight of the water-filled bottle. Then the gripper was put down on the lab table, indicating force sensed by the multi-axis forces sensor resumed to the level of holding the bottle up. Afterward, the gripper was opened to release the water bottle, leading the force to go back to zero. Noticeably, when the water bottle hit the table in the transition zone between holding the bottle up and dropping the bottle down, there was a force drop and increase from the sensor data. That was caused by the gravity loss and reaction force from the table. This phenomenon offers great evidence that

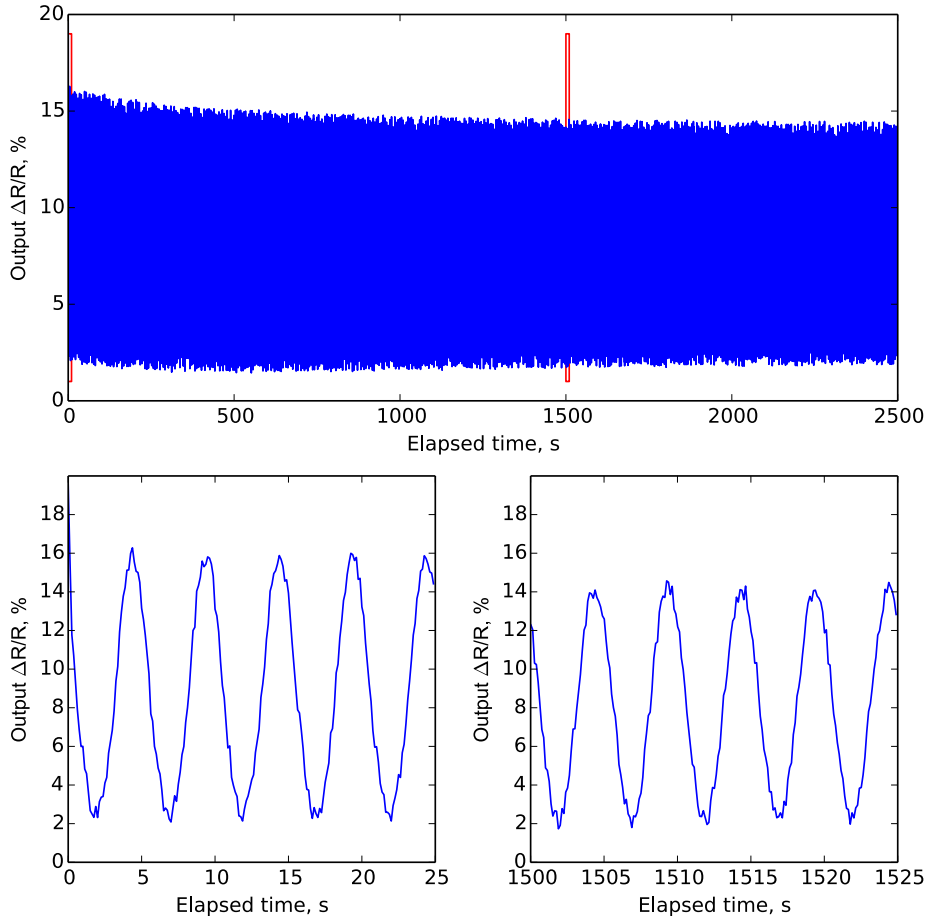

FIGURE 12. Multi-axis force sensor applied with cyclic loads (Top: repeated loading and unloading tests for 500 cycles; Bottom-left: First five cyclic data; Bottom-right: Output data after 300 cyclic loads).

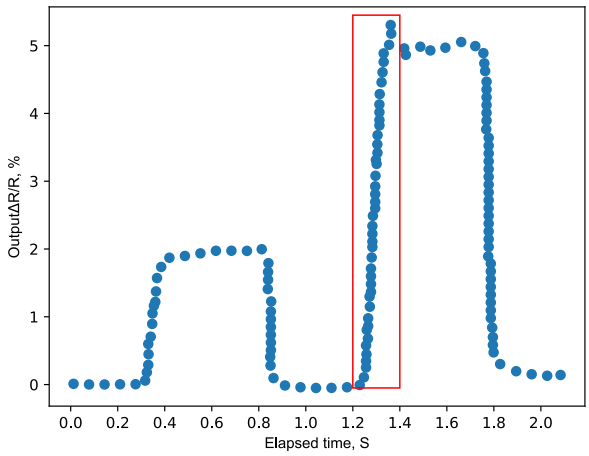

FIGURE 13. Response time tests of the multi-axis force sensor.

the fabricated force sensor demonstrated good application potential for robotic manipulation applications.

To investigate the long-term operation performance of the multi-axis force sensor, cyclic loads have been applied to the force sensor. The output data has been plotted in Fig. 12. Comparing the outputs from the initial few cyclic loads with outputs after 300 loading-unloading cycles, the results indicated hysteresis existed at the initial phase of running the sensor. However, the outputs of the sensor remained relatively stable after a few tens of cyclic loads, demonstrating a fair performance under repeated working conditions. However, for more rigorous long-term operation performance or life-span duration tests regarding the multi-axis force sensor, more tests need to be done to evaluate the reliability of the multi-axis force sensor in the future. Dynamic response of the multi-axis force sensor has been tested as shown in Fig. 13. The results demonstrated that the multi-axis force sensor achieves a dynamic response time within 200 ms, which is comparable with their counterpart in literature [35].

IV. CONCLUSION

To conclude, this work implemented a multi-axis soft sensor utilizing piezoresistive film strips cut from carbon-based piezoresistive composite Velostat. The sensing elements embedded inside the sensor are fabricated with laser ablation, which provides their uniform initial resistances and relatively lower discrepancies in terms of sensor performances. The sensor has been characterized in x, y, and z directions with

a sensitivity of 2.1%/N, 2.2%/N, and 4.2%/N, respectively, demonstrating high linearity and low crosstalk. The sensor functions are demonstrated by pressing and rubbing tests, indicating multi-axis force sensing capability. The multi-axis force sensor was also applied on a motorized robotic gripper, and tested by grasping a water-filled bottle. The multi-axis force sensor demonstrated good force sensing capability in robotic manipulation and capturing subtle object collisions during motions, shedding bright light in future robotic applications for low-cost multi-axis force measurements. Besides, the dynamic performance of the multi-axis force sensor has been tested to be within 200 ms. Future work will involve the optimization of the sensor structure and applications with the sensor array formed by multiple sensors.

ACKNOWLEDGMENT

The authors would like to thank Sheng Peng from Epic Sensor Technology Inc., for his help with transducers.

REFERENCES

[1] M.-K. Kang, S. Lee, and J.-H. Kim, "Shape optimization of a mechanically decoupled six-axis force/torque sensor," *Sens. Actuators A, Phys.*, vol. 209, pp. 41–51, Mar. 2014. [Online]. Available: https://www.sciencedirect.com/science/article/pii/S092442471400003X

[2] J. Xu and A. Song, "A miniature multiaxis force/torque sensor for acupuncture," *IEEE Sensors J.*, vol. 23, no. 7, pp. 6660–6671, Apr. 2023.

[3] A. F. Fernandez, F. Berghmans, B. Brichard, P. Mégret, M. Decréton, M. Blondel, and A. Delchambre, "Multi-component force sensor based on multiplexed fibre Bragg grating strain sensors," *Meas. Sci. Technol.*, vol. 12, no. 7, pp. 810–813, Jul. 2001, doi: 10.1088/0957-0233/12/7/310.

[4] P. Valdastri, S. Roccella, L. Beccai, E. Cattin, A. Menciassi, M. C. Carrozza, and P. Dario, "Characterization of a novel hybrid silicon three-axial force sensor," *Sens. Actuators A, Phys.*, vols. 123–124, pp. 249–257, Sep. 2005. [Online]. Available: https://www.sciencedirect.com/science/article/pii/S0924424705000129

[5] L. Wang and D. J. Beebe, "A silicon-based shear force sensor: Development and characterization," *Sens. Actuators A, Phys.*, vol. 84, nos. 1–2, pp. 33–44, Aug. 2000. [Online]. Available: https://www.sciencedirect.com/science/article/pii/S0924424799003428

[6] K. Loffler, M. Gienger, F. Pfeiffer, and H. Ulbrich, "Sensors and control concept of a biped robot," *IEEE Trans. Ind. Electron.*, vol. 51, no. 5, pp. 972–980, Oct. 2004.

[7] J. Pan, Z. Zhang, C. Jiang, L. Zhang, and L. Tong, "A multifunctional skin-like wearable optical sensor based on an optical micro-/nanofibre," *Nanoscale*, vol. 12, no. 33, pp. 17538–17544, 2020, doi: 10.1039/D0NR03446K.

[8] G. Liang, Y. Wang, D. Mei, K. Xi, and Z. Chen, "Flexible capacitive tactile sensor array with truncated pyramids as dielectric layer for three-axis force measurement," *J. Microelectromech. Syst.*, vol. 24, no. 5, pp. 1510–1519, Oct. 2015.

[9] S. D. M. Nasab, A. Beiranvand, M. T. Masouleh, F. Bahrami, and A. Kalhor, "Design and development of a multi-axis force sensor based on the Hall effect with decouple structure," *Mechatronics*, vol. 84, Jun. 2022, Art. no. 102766. [Online]. Available: https://www.sciencedirect.com/science/article/pii/S0957415822000216

[10] O. Al-Mai, M. Ahmadi, and J. Albert, "A compliant 3-axis fiber-optic force sensor for biomechanical measurement," *IEEE Sensors J.*, vol. 17, no. 20, pp. 6549–6557, Oct. 2017.

[11] B. Aksoy, Y. Hao, G. Grasso, K. M. Digumarti, V. Cacucciolo, and H. Shea, "Shielded soft force sensors," *Nature Commun.*, vol. 13, no. 1, p. 4649, Aug. 2022.

[12] P. Di Palma, E. De Vita, A. Iadicicco, and S. Campopiano, "Force sensor based on FBG embedded in silicone rubber," *IEEE Sensors J.*, vol. 23, no. 2, pp. 1172–1178, Jan. 2023.

[13] S. S. Suprapto, A. W. Setiawan, H. Zakaria, W. Adiprawita, and B. Supartono, "Low-cost pressure sensor matrix using Velostat," in *Proc. 5th Int. Conf. Instrum., Commun., Inf. Technol., Biomed. Eng. (ICICI-BME)*, Nov. 2017, pp. 137–140.

[14] A. Dzedzickis, E. Sutinys, V. Bucinskas, U. Samukaite-Bubniene, B. Jakstys, A. Ramanavicius, and I. Morkvenaite-Vilkonciene, "Polyethylene-carbon composite (Velostat®) based tactile sensor," *Polymers*, vol. 12, no. 12, p. 2905, Dec. 2020. [Online]. Available: https://www.mdpi.com/2073-4360/12/12/2905

[15] D. Chen, Y. Cai, and M.-C. Huang, "Customizable pressure sensor array: Design and evaluation," *IEEE Sensors J.*, vol. 18, no. 15, pp. 6337–6344, Aug. 2018.

[16] S. Sundaram, P. Kellnhofer, Y. Li, J.-Y. Zhu, A. Torralba, and W. Matusik, "Learning the signatures of the human grasp using a scalable tactile glove," *Nature*, vol. 569, no. 7758, pp. 698–702, May 2019.

[17] M. Hopkins, R. Vaidyanathan, and A. H. Mcgregor, "Examination of the performance characteristics of Velostat as an in-socket pressure sensor," *IEEE Sensors J.*, vol. 20, no. 13, pp. 6992–7000, Jul. 2020.

[18] A. Fatema, S. Poondla, R. B. Mishra, and A. M. Hussain, "A low-cost pressure sensor matrix for activity monitoring in stroke patients using artificial intelligence," *IEEE Sensors J.*, vol. 21, no. 7, pp. 9546–9552, Apr. 2021.

[19] L. Yuan, H. Qu, and J. Li, "Velostat sensor array for object recognition," *IEEE Sensors J.*, vol. 22, no. 2, pp. 1692–1704, Jan. 2022.

[20] S. Pohtongkam and J. Srinonchat, "Object recognition for humanoid robots using full hand tactile sensor," *IEEE Access*, vol. 11, pp. 20284–20297, 2023.

[21] C.-C. Wen and W. Fang, "Tuning the sensing range and sensitivity of three axes tactile sensors using the polymer composite membrane," *Sens. Actuators A, Phys.*, vols. 145–146, pp. 14–22, Jul. 2008. [Online]. Available: https://www.sciencedirect.com/science/article/pii/S0924424707007236

[22] K. Yellapantula, H. Devaraj, M. Assadian, L. Stuart, C.-Y. Lo, W. C. Gan, and K. Aw, "Soft and flexible sensor array using carbon black pillars for object recognition via pressure mapping," *Measurement*, vol. 159, Jul. 2020, Art. no. 107781. [Online]. Available: https://www.sciencedirect.com/science/article/pii/S0263224120303195

[23] D. M. Vogt, Y.-L. Park, and R. J. Wood, "Design and characterization of a soft multi-axis force sensor using embedded microfluidic channels," *IEEE Sensors J.*, vol. 13, no. 10, pp. 4056–4064, Oct. 2013.

[24] D. Maddipatla, X. Zhang, A. K. Bose, S. Masihi, B. B. Narakathu, B. J. Bazuin, J. D. Williams, M. F. Mitchell, and M. Z. Atashbar, "A polyimide based force sensor fabricated using additive screen-printing process for flexible electronics," *IEEE Access*, vol. 8, pp. 207813–207821, 2020.

[25] X. Zhou and W. Cao, "Flexible and stretchable carbon-based sensors and actuators for soft robots," *Nanomaterials*, vol. 13, no. 2, p. 316, Jan. 2023. [Online]. Available: https://www.mdpi.com/2079-4991/13/2/316

[26] J.-H. Kim, "Multi-axis force-torque sensors for measuring zero-moment point in humanoid robots: A review," *IEEE Sensors J.*, vol. 20, no. 3, pp. 1126–1141, Feb. 2020.

[27] J. O. Templeman, B. B. Sheil, and T. Sun, "Multi-axis force sensors: A state-of-the-art review," *Sens. Actuators A, Phys.*, vol. 304, Apr. 2020, Art. no. 111772. [Online]. Available: https://www.sciencedirect.com/science/article/pii/S0924424719308842

[28] H. Liu, X. Song, X. Wang, S. Wang, N. Yao, X. Li, W. Fang, L. Tong, and L. Zhang, "Optical microfibers for sensing proximity and contact in human–machine interfaces," *ACS Appl. Mater. Interfaces*, vol. 14, no. 12, pp. 14447–14454, Mar. 2022, doi: 10.1021/acsami.1c23716.

[29] V. K. S. Shante and S. Kirkpatrick, "An introduction to percolation theory," *Adv. Phys.*, vol. 20, no. 85, pp. 325–357, May 1971, doi: 10.1080/00018737100101261.

[30] F. Coupette, L. Zhang, B. Kuttich, A. Chumakov, S. V. Roth, L. González-García, T. Kraus, and T. Schilling, "Percolation of rigid fractal carbon black aggregates," *J. Chem. Phys.*, vol. 155, no. 12, Sep. 2021, Art. no. 124902, doi: 10.1063/5.0058503.

[31] T. Khan, M. S. Irfan, M. Ali, Y. Dong, S. Ramakrishna, and R. Umer, "Insights to low electrical percolation thresholds of carbon-based polypropylene nanocomposites," *Carbon*, vol. 176, pp. 602–631, May 2021. [Online]. Available: https://www.sciencedirect.com/science/article/pii/S0008622321001822

[32] T. Nguyen, T. Dinh, H.-P. Phan, T. A. Pham, V. T. Dau, N.-T. Nguyen, and D. V. Dao, "Advances in ultrasensitive piezoresistive sensors: From conventional to flexible and stretchable applications," *Mater. Horizons*, vol. 8, no. 8, pp. 2123–2150, 2021, doi: 10.1039/D1MH00538C.
[33] D. Benfield, S. Yue, E. Lou, and W. A. Moussa, "Design and calibration of a six-axis MEMS sensor array for use in scoliosis correction surgery," *J. Micromech. Microeng.*, vol. 24, no. 8, Aug. 2014, Art. no. 085008. [Online]. Available: https://api.semanticscholar.org/CorpusID:111303217
[34] S. Yue, Y. Qiu, and W. A. Moussa, "Packaging-induced range tunability of tactile sensors for physiological signal monitoring applications," *IEEE Trans. Compon., Packag., Manuf. Technol.*, vol. 8, no. 4, pp. 588–596, Apr. 2018.
[35] A. A. Laaraibi, G. Jodin, D. Hoareau, N. Bideau, and F. Razan, "Flexible dynamic pressure sensor for insole based on inverse viscoelastic model," *IEEE Sensors J.*, vol. 23, no. 7, pp. 7634–7643, Apr. 2023.

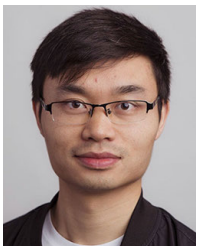

SHICHAO YUE (Member, IEEE) received the B.S. and M.Sc. degrees in mechanical manufacturing and automation from Shandong University, China, in 2009 and 2012, respectively, and the Ph.D. degree in mechanical engineering from the University of Alberta, Canada, in 2018. He is currently an Assistant Professor with the Mechanical Engineering Department, Southeast University, China. His research interests include NEMS/MEMS, intelligent sensing, and manufacturing systems.

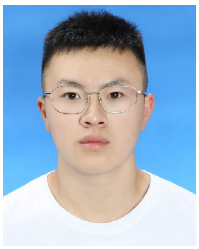

MINZHI XU is currently pursuing the B.S. degree in mechanical manufacturing and automation with Southeast University, Nanjing, China. His research interests include optics and intelligent systems.

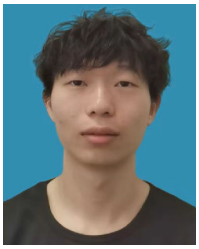

YANPENG GU is currently pursuing the B.S. degree in mechanical manufacturing and automation with Southeast University, Nanjing, China. His research interests include robotics and sensors.

WALIED MOUSSA received the B.S. and M.Sc. degrees from The American University in Cairo, Cairo, Egypt, in 1991 and 1993, respectively, and the Ph.D. degree from Carleton University, Ottawa, ON, Canada, in 2000. He is currently a Professor with the University of Alberta, Edmonton, AB, Canada, with co-appointment to the Department of Mechanical Engineering, Biomedical Engineering, and Surgery. His research interests include microelectromechanical systems (MEMS) and nanoelectromechanical systems (NEMS) research and development for the biomedical, aerospace, mechanical, and environmental fields. His research work involves both experimental and numerical approaches to these areas. He was the Chair of the International Conference MEMS, NEMS, and Smart Systems, from 2003 to 2006.